A COMPARISON OF OBJECT-BASED AND PIXEL-BASED APPROACHES TO ESTIMATE LIDAR-MEASURED FOREST CANOPY HEIGHT USING QUICKBIRD IMAGERY

Commission VI, WG VI/4

G. Chen [a, *], G. J. Hay [a], G. Castilla [a], B. St-Onge [b], R. Powers [a]

[a] Department of Geography, University of Calgary, 2500 University Dr., Calgary, AB, T2N 1N4 Canada - gangchen@ucalgary.ca

[b] Department of Geography, Université du Québec à Montréal, C.P. 8888, succ. Centre-Ville, QC, H3C 3P8 Canada -

KEY WORDS: Canopy height, Geographic object-based image analysis (GEOBIA), Geographic object-based texture (GEOTEX), Tree-ray-shadow geometry (TG), Quickbird, Lidar

ABSTRACT:

Canopy surface height (CSH) is a significant forest biophysical parameter to estimate above-ground biomass and carbon content. High- spatial resolution optical remotely sensed data have shown promising results to delineate various forest biophysical properties; though few studies have evaluated the accuracy of forest height information from such data. In this study, we compare several strategies using high-resolution Quickbird imagery to estimate CSH measured from small-footprint lidar data in a forest scene. Two main approaches were tested: 1) geographic object-based image analysis (GEOBIA), where the areal units are the objects from a segmentation-derived partition, which are akin to *forest patches*; and 2) pixel-based, where the areal units used to estimate CSH are the cells of a grid-shaped partition, which are akin to *square field plots*. Multiple linear regression models between *within areal unit spectral response* and *lidar-measured CSH* were developed for these two types of approaches using various *areal unit sizes* (AUSs). The best results (derived from the optimal AUSs) illustrated a better fitting model employing the GEOBIA approach (R^2 = 0.605, RMSE = 2.86 m) than the pixel-based approach (R^2 = 0.544, RMSE = 2.97 m). To develop more representative models when using their optimal AUSs, texture (i.e., standard deviation, skewness and kurtosis) and tree-ray-shadow geometry were investigated and applied to GEOBIA and pixel-based approaches. For the GEOBIA approach, the addition of texture and tree-ray-shadow geometry explained more variance of lidar-measured CSH by 5 percent and 10 percent respectively. The best performance (R^2 = 0.739, RMSE = 2.60 m) was achieved using the combination of all three types of variables. For the pixel-based approach, only slight improvements were made with the best result (R^2 = 0.577, RMSE = 2.88 m) achieved using all types of variables in the regression analysis. The comparisons in this study illustrate the potential of using meaningful image-objects instead of traditional fixed-size square grids to achieve higher accuracies in estimating the vertical structure of tree canopies.

1. INTRODUCTION

Forests play an important role in the global carbon budget because they dominate the dynamics of the terrestrial carbon cycle (Dong *et al*., 2003), for example, 90% of above-ground carbon is stored in tree stems (Hese *et al*., 2005). As a signatory of the Kyoto Protocol and a guardian of approximately 10% of global forests, Canada has committed to produce accurate estimates of its forest's carbon content. Since forest vertical structure (e.g., height) - a significant component of forest inventories - is highly correlated with above-ground biomass and therefore carbon content (Lefsky *et al*., 2002), an accurate and efficient measurement of forest height is crucial to the success of carbon estimation.

Lidar (*light detection and ranging*), a relatively recent remote sensing tool, has demonstrated the ability to provide highly accurate information on forest vertical structure (Lim *et al*., 2003). Compared with satellite data acquisition, lidar data collection and processing are expensive, typically covering only small sites (e.g., narrow transects); however larger provincial and state-wide acquisition programs are currently being developed. Optical remote sensing imagery provide a continuous view of broad areas with a relatively low cost, especially for high-spatial resolution imagery (<5.0m) (hereafter *H-res*), which have shown promising results to estimate various forest biophysical properties, such as stand density, age and tree species composition (Wulder *et al.*, 2004). In addition, a number of studies have evaluated the accuracy of forest height information from H-res optical data. Franklin and McDermid (1993) found a significant correlation between H-res CASI (Compact Airborne Spectrographic Imager) red band and forest height at the *stand* level (R = 0.75). Hyde *et al.* (2006) compared different types of remotely sensed data to map forest structure for wildlife habitat analysis and found a R^2 of 0.566 while using Quickbird imagery to estimate mean canopy height. Similarly, Donoghue and Watt (2006) used IKONOS data to estimate lidar-measured forest height for densely stocked plantation areas in northern England. They found lidar and IKONOS data appear to show good agreement with trees less than 10 m in height. However, height predictions were very poor above 10 m.

For almost three decades, traditional pixel-based image processing approaches have been applied to medium resolution remotely sensed data, because individual pixels - the basic study

* Corresponding author.

units - were capable of characterizing different land-cover classes (Castilla and Hay, 2008). However, the spatial patterns of the objects composed by pixels were neglected, especially for H-res imagery. Recently, there has been a shift from pixel-based approaches to object-based approaches, which combine spatial and spectral information to define *image-objects* (i.e., groups of pixels that represent meaningful entities in the real world scene), instead of pixels as their basic unit. To emphasize object-based image analysis in the geographical domain, the name of *GEOgraphic Object-Based Image Analysis* (GEOBIA) was proposed by Hay and Castilla (2008). Advantages of GEOBIA approaches over pixel-based approaches have been shown in several forest studies. For example, in early work, Hay *et al*. (1996) presented an object-based adaptive triangulated primitive neighborhood method (TPN) applied on H-res CASI imagery to extract forest structural texture. This improved the overall classification accuracy to 78% versus the classification generated from the pixel-based grey level co-occurrence matrix (GLCM) approach (35%). Another study to estimate vegetation parameters (i.e., above-ground biomass and leaf area index) also showed that object-based parameter estimation performed better than per-pixel estimation (Addink *et al*., 2007).

Lidar data have proven their ability to accurately estimate forest vertical structure. However, the high cost of data collection and processing typically confine the use of lidar systems to relatively small areas. In this study, we hypothesize that H-res optical data (which have been used to estimate forest biophysical properties at a relatively low cost), can be combined with profiling lidar data to spatially extend forest height information from small areas to large areas. A prerequisite to this hypothesis is that a high R^2 must be obtained between lidar-measured canopy height and optical variables. In this study, our first objective is to (i) examine the potential of using H-res Quickbird imagery to estimate *canopy surface height* (CSH) measured from small-footprint lidar data covering the same study area. Our second objective is to (ii) develop and compare two types of CSH estimation models using pixel-based and GEOBIA approaches. (iii) Our third objective is to investigate if an optimal areal unit size (AUS) exists for these approaches.

2. METHODS

2.1 Study area

The study area (49°52'N, 125°20'W) is located approximately 10 km southwest of Campbell River on the east coast of Vancouver Island, British Columbia, Canada (Figure 1). The forest types are dominated by Douglas-fir [*Pseudotsuga menziesii* (Mirb.) Franco] of 80%+, with small proportions of Western Red Cedar [*Thuja plicata* (Donn.)], Western Hemlock [*Tsuga heterophylla* (Raf.) Sarg.] and Red Alder (*Alnus rubra* Bong.). This study is performed over a 2.5 × 2.5 km (625 ha) area, where most forest stands consist predominantly of regenerating forest from harvest and are between 20-60 years of age.

2.2 Field data

This study area has been the subject with a relatively large campaign in Coops *et al*. (2007), who investigated the ability of using the same small-footprint lidar data to estimate mean canopy height. Six 20 × 20 m square plots were selected in six separate stands covering the range of Douglas-fir structural stage conditions. They compared field measured plot height and lidar measured height and obtained a R^2 of 0.85 and a standard error of 1.8 m.

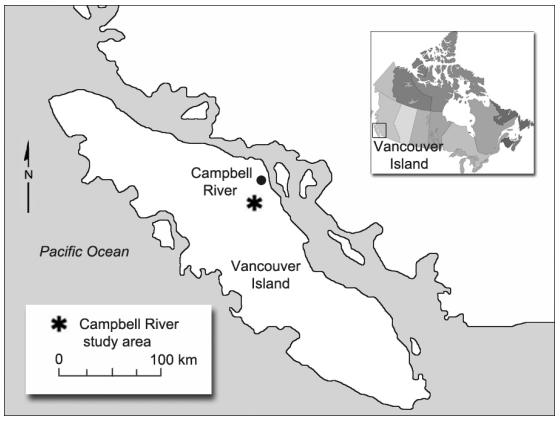

Figure 1. Study area located southwest of Campbell River, Vancouver Island, Canada

2.3 Lidar data

Lidar data were acquired June 8, 2004, by the Terrain Scanning Lidar system (Terra Remote Sensing Inc., Sidney, Canada) on a Bell 206 Jet Ranger helicopter. Terrain Scanning Lidar is a discrete return lidar system (Lightwave Model 110) with a pulse repetition frequency of 10 kHz, a wavelength of 1047 nm, a swath width of 56°, and a beam divergence of 3.5 mrad. This mission used a continuous scanning mode in a typical zigzag pattern, yielding point densities of 0.7/m^2 and a footprint size of 0.19 m.

The raw lidar point cloud data were derived containing both ground and non-ground returns. In this study, non-ground points were assumed equivalent to the returns from tree canopy, because no artificial objects exist in the study site. Classifying point cloud data into ground and tree canopy returns was implemented in the software of Terrascan v4.006 (Terrasolid, Helsinki, Finland). Ground and tree canopy returns were then separately interpolated to form a digital terrain model (DTM) and a digital surface model (DSM) with 1 m grid cell size. The final step was to create the canopy height model (CHM), which was generated by subtracting DEM from DSM.

2.4 Quickbird data

A cloud-free Quickbird image was acquired August 11, 2004 over the same study area. This image consists of four multispectral bands [i.e., blue, green, red and near infrared (NIR) bands] and one panchromatic band. A geometric correction was performed using a coarse DEM when the image was ordered at the standard product level. The different spatial resolutions between the Quickbird and lidar data made for a difficult comparison. Therefore, a PC spectral sharpening technique (Welch and Ahlers, 1987) was used to rescale the Quickbird image to a 1 m spatial resolution multispectral image by fusing multispectral bands with the panchromatic band. The Quickbird image was then geometrically co-registered to lidar data using 105 ground control points. A 2nd degree polynomial warping method and nearest neighbor resampling were selected in co-registration, yielding the RMSE of 0.65 m.

2.5 Data analysis

2.5.1 Pixel-based approach

Since all regression models were developed to estimate lidar-measured CSH using Quickbird imagery, independent variables were derived from Quickbird data, while the dependent variable (i.e., CSH) was measured from the lidar CHM. The basic areal units for the pixel-based approach are the cells of a grid-shaped partition, which are akin to contiguous square field plots. Independent variables included spectral responses [i.e., digital numbers (DNs)], image-texture [i.e., standard deviation (SD), skewness and kurtosis] and tree-ray-shadow geometry (TG), which were extracted and averaged within each grid cell.

Variables (Pixel-based)	Variables (GEOBIA)	Description
Spectral Response		
▪ DN*i*_Pix	DN*i*_Obj	DNs for the *i*th band
Image-texture		
▪ SD*i*_Pix	SD*i*_Obj	SD for the *i*th band
▪ SK*i*_Pix	SK*i*_Obj	Skewness for the *i*th band
▪ KU*i*_Pix	KU*i*_Obj	Kurtosis for the *i*th band
Tree-ray-shadow Geometry (TG)		
▪ TG_Pix	TG_Obj	TG for the NIR band

Table 1. Variables extracted from Quickbird imagery

As Table 1 shows, DNs were calculated from pan-sharpened (1 m pixel size) Quickbird multispectral bands (i.e., blue, green, red and NIR). Image-texture plays an important role in forest landscapes as well. Especially for H-res remote sensing imagery, texture, which normally refers to a statistical measurement of the spatial variability of neighbouring pixels within a fixed window assessed across the image, can provide valuable tree structure information in forest studies. Generally, subjective decisions to define square kernel sizes are made in pixel-based texture analysis. The grid-shaped cells with a range of sizes were chosen as the square texture windows in this study (Figure 2). To make a straightforward comparison between pixel-based and GEOBIA approaches, only the first-order texture measures of SD, skewness and kurtosis were applied to four spectral bands in this study (Equations 1, 2 and 3).

$$SD_i = \sqrt{\frac{1}{N-1}\sum_{j=1}^{N}(x_{ij}-\mu_i)^2} \quad (1)$$

$$SK_i = \frac{1}{(N-1)SD_i^3}\sum_{j=1}^{N}(x_{ij}-\mu_i)^3 \quad (2)$$

$$KU_i = \frac{1}{(N-1)SD_i^4}\sum_{j=1}^{N}(x_{ij}-\mu_i)^4 - 3 \quad (3)$$

where SD_i = SD of the texture window in the ith band
x_{ij} = value of the pixel j in the ith band
μ_i = mean value of the texture window in the ith band
N = number of pixels in the texture window
SK_i = skewness of the texture window in the ith band
KU_i = kurtosis of the texture window in the ith band

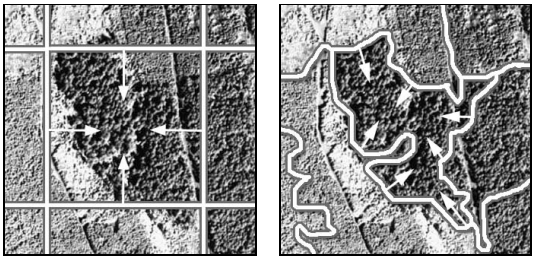

Figure 2. A typical forest area using square windows (left) and object-based windows (right) to extract texture

Shadow effects are becoming more obvious and attractive with the emergence of H-res optical remote sensing imagery. In forests, variables of CSH, tree shadow fraction and stem density are highly correlated due to the relationship between trees, sun's rays and shadows (Figure 3). When stem density is fixed, higher CSH typically has larger crown diameter and causes a larger shadow fraction. Similarly, if shadow fraction remains the same, higher CSH means lower stem density in the study site. Therefore, the variable of TG calculated by dividing shadow fraction by stem density was applied to estimate CSH. Specifically, shadow fraction was derived using two steps: (i) a visually defined threshold was used to separate the Quickbird NIR band into shaded and non-shaded pixels, and (ii) the ratio between the number of shaded pixels and all pixels within each areal unit was applied to the shadow fraction. Stem density was calculated by the following steps: (i) the mean filter, using a window size of 3 by 3 pixel, was applied to remove image noise, (ii) the local maximum algorithm, using a window size of 3 by 3 pixel, was applied to extract all tree tops, and (iii) the ratio between the number of tree tops and all pixels within each areal unit was applied to stem density.

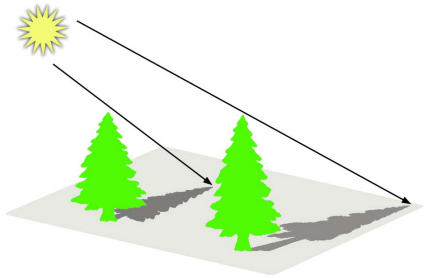

Figure 3. The relationship between trees, sun's rays and shadows

The lidar-measured dependent variable CSH was obtained from the lidar CHM. Similar to the extraction of independent variables, CSH for each cell was calculated by averaging all height values within the cell extent.

2.5.2 GEOBIA approach

The basic areal units for the GEOBIA approach are the objects (i.e., segments) of a segmentation-derived partition, which are akin to forest patches. The Definiens Professional 5 (Definiens Imaging GmbH, Munich, Germany) multi-resolution segmentation software was applied on the pan-sharpened multispectral Quickbird imagery to create image-objects. The characteristics of similarity and heterogeneity for each object are controlled using four parameters, color, shape, smoothness and compactness. Software default values of 0.7 and 0.3 were used for color and shape. To obtain smoother boundaries for forest segments, smoothness and compactness were set as 0.8 and 0.2, respectively. All four spectral bands were assigned the same weight during the segmentation.

In order to compare the GEOBIA approach with the pixel-based approach in lidar-measured CSH estimation, similar variables were extracted for the GEOBIA approach (Table 1). However, all variables were extracted from objects instead of grid-shaped cells. The name - *geographic object-based texture* (GEOTEX) is used to describe texture extracted from image-objects (Figure 2). It should be noted, traditional pixel-based texture analysis (e.g., GLCM) normally uses square moving windows to extract texture, which cannot fully characterize the real forest landscape. This is primarily because image-objects (e.g., individual trees or tree clusters) in forests generally represent highly variable shapes that are difficult to describe using square texture windows. With GEOBIA, these boundaries can automatically represent image-object edges, thus GEOTEX measures derived from the inner pixels of objects are more reliable. The lidar-measured dependent variable CSH was also obtained from lidar CHM by averaging all height values within each object extent.

2.6 Models and AUSs

2.6.1 Pixel-based approach

Multiple linear regression models were developed using Quickbird-derived independent variables to estimate lidar-measured CSH. To avoid the overfitting problem in models, correlation coefficients were first calculated between all variables. Independent variables were retained under two rules: (i) variables having correlations lower than 0.7 and (ii) the variable having a higher correlation with CSH in case two variables had a correlation of 0.7 or higher with each other. Then a stepwise method was used in the regression analysis to develop models, which were performed at a 0.05 level of significance. The whole study area was partitioned into discrete non-overlapping areal units in the form of grid-shaped cells. The models were developed using all the cells.

The *leave-one-out cross-validation* technique was applied for model validation. In this study case, validation was performed each time using one unit as the validation sample and the remaining units as the training data each time to estimate the residual between model predicted CSH and lidar-measured CSH. This step was repeated until each unit was used once as the validation sample. All residuals were used to calculate a RMSE for each validated model. Consequently, the R^2 and RMSE were selected to evaluate the accuracy of our models.

The pixel-based approach was performed using 14 different levels of AUSs, 0.010 ha (10×10 m), 0.040 ha (20×20 m), 0.160 ha (40×40 m), 0.360 ha (60×60 m), 0.640 ha (80×80 m), 1.000 ha (100×100 m), 1.440 ha (120×120 m), 1.960 ha (140×140 m), 2.403 ha (155×155 m), 2.890 ha (170×170 m), 3.610 ha (190×190 m), 4.410 ha (210×210 m), 5.290 ha (230×230 m) and 6.503 ha (255×255 m) from plot levels to stand levels. To ascertain the optimal AUS, fitting models were developed at all 14 levels separately. In order to simplify the comparison between pixel-based and GEOBIA approaches, only spectral responses were used to determine the optimal AUSs for these two types of approaches. Then the performances of texture and TG in the regression models were examined using the optimal AUS for each approach.

2.6.2 GEOBIA approach

Similar to the pixel-based approach, multiple linear regression models were developed for the GEOBIA approach using Quickbird-derived variables to estimate lidar-measured CSH. Independent variables were obtained under the same rules as they were mentioned in section 2.6.1. Moreover, a stepwise method was also applied in the regression analysis at a 0.05 level of significance. All objects were used in the regression analysis.

The leave-one-out cross-validation technique was applied for model validation as well. However, RMSE was calculated in a different way. Unlike the pixel-based approach, where all samples (i.e., grid-shaped cells) have the same size for each level of AUS, image-objects in the GEOBIA approach are of varying sizes and shapes even at the same scale. Therefore, an area-weighted RMSE, where each object was considered based on the size of its area, was obtained using the following equation:

$$RMSE_{Area-weighted} = \sqrt{\frac{1}{A_N}\sum_{i=1}^{N}[A_i(CSH_{QB\_i} - CSH_{Lidar\_i})^2]} \quad (4)$$

where CSH_{QB_i} = CSH calculated from the regression using Quickbird imagery for the *i*th object

CSH_{Lidar_i} = CSH measured from lidar data for the *i*th object

A_i = area for the *i*th object

A_N = area for the whole study area (i.e., 625 ha in this study)

N = number of objects

In order to be comparable with the AUSs used for the pixel-based approach, 14 different values of mean object size (MOS) (0.011 ha, 0.060 ha, 0.151 ha, 0.332 ha, 0.640 ha, 0.994 ha, 1.454 ha, 1.990 ha, 2.332 ha, 2.741 ha, 3.511 ha, 4.371 ha, 5.165 ha and 6.579 ha) were chosen and then translated into scale parameters in Definiens Professional 5 segmentation software.

3. RESULTS AND DISCUSSION

3.1 Optimal Areal Unit Sizes (AUSs)

Figure 3 shows the trends of R^2 values for both pixel-based and GEOBIA approaches with various AUSs. To simplify the comparison and ascertain the optimal AUSs for the two approaches, only spectral responses were used in the regression analysis. As the cell size and the MOS increase using relatively small AUSs (i.e., smaller than 0.500 ha), R^2 values of both approaches increase rapidly. However, two different styles of changing lines were generated using relatively large AUSs (i.e., larger than 0.500 ha). For the pixel-based approach, the R^2 value increases slightly before it reaches the maximum value of 0.544 using an AUS of 1.000 ha. Then it decreases slightly using cell sizes from 1.000 ha to 6.503 ha. For the GEOBIA approach, the R^2 value significantly increases from 0.393 to 0.605 in the similar range of AUSs (from 0.640 ha to 6.579 ha). The maximum R^2 value of 0.605 was obtained using the AUS of 6.579 ha.

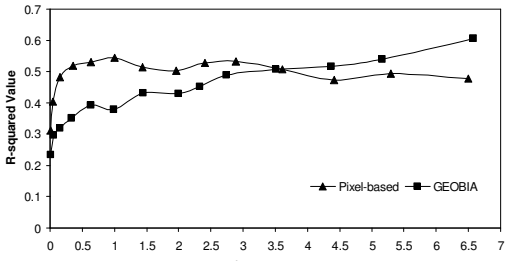

Figure 3. A comparison of R^2 values derived from 14 different levels of AUSs using pixel-based and GEOBIA approaches

It should be noted that, there is a threshold using the AUS of approximately 3.600 ha, where pixel-based and GEOBIA approaches have the similar performance, with a R^2 of approximately 0.510 (Figure 3). When the AUSs used in both approaches are smaller than this threshold, the pixel-based approach can explain more variance of CSH. However, a steady increase of the R^2 makes the GEOBIA approach more accurate to estimate CSH when larger AUSs (than the threshold) were applied. This indicates that it is appropriate to use a small size of grid-shaped cells for the pixel-based approach in this study area, while large objects are more suitable in the GEOBIA approach. This condition may be caused by the forest shadows in H-res remote sensing imagery. When relatively small AUSs are used, shaded and sunlit image-objects are grouped separately, which cause a high variation between various objects to estimate CSH. However, pixel-based approaches average the values of DNs in the grid-shaped partitions, which reduce the shadow effect and decrease the variation. When relatively large objects are used, objects derived from GEOBIA approaches can dramatically increase the accuracy because (i) the objects are more reasonable to cover the real forest patches compared to grid cells derived from pixel-based approaches and (ii) shaded and sunlit portions are grouped together to reduce the shadow effects. In the case of this study area, the GEOBIA approach has a relatively better performance (R^2 = 0.605, RMSE = 2.86 m) than the pixel-based approach (R^2 = 0.544, RMSE = 2.97 m) using their optimal AUSs (Table 2).

Approach	AUS (ha)	R^2	RMSE (m)	Model
Pixel-based	1.000	0. 544	2.97	37.9170-0.1939*DN3_Pix
GEOBIA	6.579	0. 605	2.86	32.6604-0.1321*DN3_Obj

Table 2. Best fitting models (derived from the optimal AUSs) using pixel-based and GEOBIA approaches

3.2 Model Performance of Image-texture and Tree-ray-shadow Geometry (TG)

Regression models only using spectral responses derived from remote sensing imagery to estimate forest biophysical parameters have been widely applied in forest studies. However, texture and TG, which consider the spatial and spectral relationships within each areal unit, can provide more valuable information to improve the CSH estimation accuracy. Results in Table 3 show that the accuracy of each model using either a pixel-based or GEOBIA approach is improved by the addition of texture and TG variable. However, only slight improvements were made using different variable combinations for the pixel-based approach (Tables 3). Compared to the models only using DNs, the best result (R^2 = 0.577, RMSE = 2.88 m), which was obtained by applying all three types of variables in the regression analysis, can only explain ≈ 3 percent more variance of lidar-measured CSH. For the GEOBIA approach, the addition of GEOTEX helps the GEOBIA approach explain 65.4 percent variance of the lidar-measured CSH. Additionally, spectral responses together with TG bring a significant 11.4 percent improvement of R^2 with an RMSE of 2.73 m. Similar to the pixel-based approach, the best performance (R^2 = 0.739, RMSE = 2.60 m) was achieved using the combination of all three types of variables. All models developed for the GEOBIA approach are more accurate than the models developed for the pixel-based approach with an exception of low RMSE of 3.07 m when both spectral responses and GEOTEX were applied in the GEOBIA approach. The results in this study indicate that the variables of GEOTEX and TG (depending on appropriate kernel sizes and shapes), perform better in the GEOBIA approach than the pixel-based approach. This is especially true for the variable of TG (which extracts the spatial relationships between trees, and the sun's rays and shadows from image-objects tree-ray-shadow geometry).

Figure 4 is the scatter plot of residual values for the best fitting model (i.e., highest R^2 values and lowest RMSE) using the GEOBIA approach. Similar to the calculation of area-weighted RMSE, an area-weighted residual value was used for each object. Since the optimal AUS is 6.579 ha, each residual value was multiplied by a ratio between the object size and 6.579 to obtain the final area-weighted residual value. The study area is dominated by approximately 78.7 percent of forest objects with

Approach	Variable Inputs	R^2	RMSE (m)	Variables Used in the Model
Pixel-based	▪ Spectral Response + Image-texture: DN*i*_Pix, SD*i*_Pix SK*i*_Pix, KU*i*_Pix	0.573	2.89	DN3_Pix, SD4_Pix, SK1_Pix
	▪ Spectral Response + TG: DN*i*_Pix, TG_Pix	0.570	2.89	DN3_Pix, TG_Pix, DN4_Pix
	▪ Spectral Response + Image-texture + TG: DN*i*_Pix, SD*i*_Pix, SK*i*_Pix, KU*i*_Pix, TG_Pix	0.577	2.88	DN3_Pix, SK1_Pix, SD4_Pix, TG_Pix
GEOBIA	▪ Spectral Response + GEOTEX: DN*i*_Obj, SD*i*_Obj SK*i*_Obj, KU*i*_Obj	0.654	3.07	DN3_Obj, KU2_Obj
	▪ Spectral Response + TG: DN*i*_Obj, TG_Obj	0.719	2.73	DN3_Obj, TG_Obj, DN4_Obj
	▪ Spectral Response + GEOTEX + TG: DN*i*_Obj, SD*i*_Obj, SK*i*_Obj, KU*i*_Obj, TG_Obj	0.739	2.60	DN3_Obj, TG_Obj, KU2_Obj, DN4_Obj

Table 3. Best fitting models (derived from the optimal AUSs) with different variable combinations using pixel-based and GEOBIA approaches

the mean CSH ranging between 19 m and 30 m. The regression trend line shows a threshold of 23 m in the CSH estimation. When CSH is in the range between 19 m and 23 m, the model appears more likely to overestimate lidar-measured canopy height. Conversely, the underestimation of canopy height is more likely to occur when CSH is in the range between 23 m and 30 m.

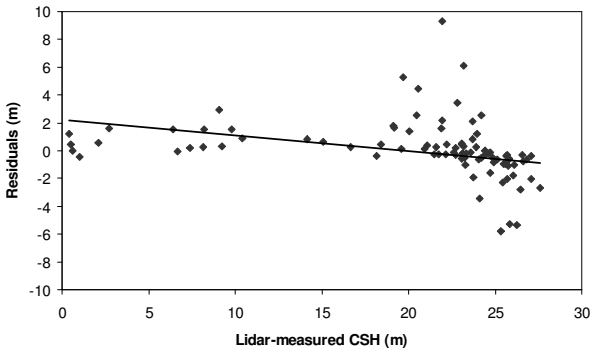

Figure 4. Scatter plot of estimated CSH versus lidar-measured CSH for the best fitting model using the GEOBIA approach

4. CONCLUSION

In this study, we investigated the potential of using high-spatial resolution Quickbird imagery to estimate canopy surface height (CSH) measured from small-footprint lidar data in a forest scene. We compared the results from pixel-based and GEOBIA approaches. The best performance was achieved from the GEOBIA approach (R^2 = 0.739, RMSE = 2.60 m), which might be used to facilitate the practical application of forest management, such as the relatively accurate and efficient delineation of forest inventory polygons.

The results in this study also show that an appropriate AUS (e.g., grid cell size or mean object size) plays an important role in CSH estimation for both pixel-based and GEOBIA approaches, though the pixel-based approach is less sensitive to various AUSs when the AUS is larger than a certain threshold. An arbitrary decision of the AUS can cause a low-accuracy result, even though the correct approach is applied. This relates to the Modifiable Areal Unit problem (MAUP), but is beyond the scope of this letter.

Although spectral responses (i.e., DNs) are the measures directly derived from remote sensing platforms, we note that image-texture (i.e., SD, skewness and kurtosis) and tree-ray-shadow geometry (TG) extracted from spectral responses also provide useful spatial and spectral information, which help our models explain more variance and achieve less RMSE of the forest vertical structure. Especially for the GEOBIA approach, variables of texture and TG calculated from image-objects instead of grid-shaped cells have proven to be more reasonable and accurate in characterizing the real forest landscape.

5. REFERENCES

Addink, E. A., de Jong, S. M. and Pebesma, E. J., 2007. The importance of scale in object-based mapping of vegetation parameters with hyperspectral imagery. *Photogrammetric Engineering & Remote Sensing*, *73*, 905–912.

Castilla, G. and Hay, G. J., 2008. Image objects and geographic objects. In: Blaschke, T., Lang, S., Hay, G. J. (eds) *Object-Based Image Analysis - Spatial concepts for knowledge-driven remote sensing applications*., Chapter 1.5. pp. 97-112 Springer. 700 p.

Coops, N. C., Hilker, T., Wulder, M. A., St-Onge, B., Newnham, G., Siggins, A. and Trofymow, J. A., 2007. Estimating canopy structure of Douglas-fir forest stands from discrete-return LiDAR. *Trees - Structure and Function*, *21*, 295–310.

Dong, J., Kaufmann, R.K., Myneni, R.B., Tucker, C.J., Kauppi, P.E., Liski, J., Buermann, W., Alexeyev, V. and Hughes, M.K., 2003. Remote sensing estimates of boreal and temperate forest woody biomass: carbon pools, sources, and sinks. *Remote Sensing of Environment*, *84*, 393-410.

Donoghue, D. N. M. and Watt, P. J., 2006. Using LiDAR to compare forest height estimates from IKONOS and Landsat ETM+ data in Sitka spruce plantation forests. *International Journal of Remote Sensing*, *27*, 2161 – 2175.

Franklin, S. E. and McDermid, G. J., 1993. Empirical relations between digital SPOT HRV and CASI spectral response and lodgepole pine (*Pinus contorta*) forest stand parameters. *International Journal of Remote Sensing*, *14*, 2331 – 2348.

Hay, G. J. and Castilla, G., 2008. Geographic Object-Based Image Analysis (GEOBIA). In: Blaschke, T., Lang, S., Hay, G. J. (eds) *Object-Based Image Analysis - Spatial concepts for knowledge-driven remote sensing applications*. Chapter 1.4, pp. 81- 92 Springer. 700 p.

Hay, G. J., Niemann, K. O. and McLean, G. F., 1996. An object-specific image-texture analysis of H-resolution forest imagery. *Remote Sensing of Environment*, *55*, 108–122.

Hese, S., Lucht, W., Schmullius, C., Barnsley, M., Dubayah, R., Knorr, D., Neumann, K., Riedel, T. and Schroter, K., 2005. Global biomass mapping for an improved understanding of the CO_2 balance--the Earth observation mission Carbon-3D. *Remote Sensing of Environment*, *94*, 94-104.

Hyde, P., Dubayah, P., Walker, W., Blair, J. B., Hofton, M. and Hunsaker, C., 2006. Mapping forest structure for wildlife habitat analysis using multi-sensor (LiDAR, SAR/InSAR, ETM+, Quickbird) synergy. *Remote Sensing of Environment*, *102*, 26–36.

Lefsky, M. A., Cohen, W. B., Harding, D. J., Parkers, G. G., Acker, S. A. and Gower, S. T., 2002. Lidar remote sensing of above-ground biomass in three biomes. *Global Ecology & Biogeography*, *11*, 393-399.

Lim, K., Treitza, P., Wulder, M., St-Onge., B. and Flood, M., 2003. LiDAR remote sensing of forest structure. *Progress in Physical Geography*, *27*, 88–106.

Welch, R. and Ahlers, W., 1987. Merging Multiresolution SPOT HRV and Landsat TM Data. *Photogrammetric Engineering & Remote Sensing*, *53*, 301–303.

Wulder, M. A., Hall, R. J., Coops, N. C. and Franklin, S. E., 2004. High Spatial Resolution Remotely Sensed Data for Ecosystem Characterization. *BioScience*, *54*, 511-521.